Engineering Geology 171 (2014) 1–10

Contents lists available at ScienceDirect

Engineering Geology

journal homepage: www.elsevier.com/locate/enggeo

Mechanics and response of a surface rock block subjected to pressure fluctuations: A plucking model and its application

Yii-Wen Pan *, Kuo-Wei Li, Jyh-Jong Liao

Department of Civil Engineering, National Chiao Tung University, Taiwan

ARTICLE INFO

Article history:
Received 23 June 2013
Received in revised form 23 December 2013
Accepted 24 December 2013
Available online 2 January 2014

Keywords:
Jointed rock masses
Plucking
Scour hole
Plunge pool
Uplift
Rock riverbed

ABSTRACT

Plucking (removal of rock blocks) is often the dominant mechanism for producing a scour hole on riverbeds comprised of heavily jointed rock masses being subjected to pressure fluctuations from a jet flow. This paper explores the mechanics and response of a surface block subjected to pressure fluctuations. First a particle-flow simulation was conducted to demonstrate how repeated pressure fluctuations are able to gradually remove rock bridges in discontinuities surrounding a rock block, if a pressure fluctuation's intensity is substantial. As a consequence, these weak planes may become fully persistent. The block's uplift speed then depends on the pressure differences on the opposite (horizontal) faces, and the frictional resistance of the lateral discontinuities. This paper proposes a theoretical framework to model the mechanics and response of a rock block subjected to a sinusoidal pressure fluctuation. This model can be applied to estimate the development of a scour hole, through plucking, during a specific flood event. An example demonstrates the applicability of the proposed approach in predicting the potential depth of the scour hole.

1. Introduction

Rock is generally considered to be an erosion resistant geo-material, yet during severe floods, significant incisions, or retreating banks, may be observed in riverbeds comprised of soft rock or heavily jointed rock masses. This is especially the case when the jet flow passes a man-made spillway or natural knickpoint with a large elevation drop. Then a scour hole is very likely to be created in the plunge pool or in the riverbed downstream. This is cause for concern in regard to the stability of structures or channel morphology.

The rapid evolution of the Ta-An River channel in central Taiwan is a typical example of severe erosion in a rocky riverbed. Here an incision of around twenty meters or so has developed in just a single decade (Cook et al., 2013 Huang et al., 2013;). The unusually high rate of the knickpoint's annual retreat (up to one hundred meters) was responsible for the rapid channel incision in the Ta-An River. When it is out of control, this kind of severe incision may seriously damage the structural stability of cross-river structures, or the levees along its banks.

Whipple et al. (2000) pointed out that the mechanisms for a riverbed's erosion may include: bed shear, saltation abrasion, cavitation, plucking, and others. For a rock bed without dense joints, any one of the first three types of mechanisms may dominate, depending on the characteristics of flow conditions. Usually, the erosion rate caused by these mechanisms is relatively slow. However, when the joint spacing of rock masses is sub-meter, plucking may become the major erosion mechanism on a riverbed's heavily jointed rock masses (Whipple et al., 2000). Annandale (1995) illustrated complicated processes involving plucking, including: rock weathering; wedging by sand grains, crack propagation and dislodgement by water current. Furthermore, the complex interaction between the block matrix and water flow makes it difficult to model the plucking phenomenon in detail.

Most models for predicting erosion rates are based on rational models calibrated from field data or laboratory flume tests (Shepherd and Schumm, 1974; Wohl and Ikeda, 1997; Robinson and Hanson, 2001). These types of models are not generally derived on the basis of mechanics. A few semi-analytical models for evaluating the depth of scour holes in rock riverbeds were proposed in the past (e.g., Spurr, 1985; Akhmedov, 1988; Liu, 2005), but were not intended for modeling the plucking behavior in fractured rock masses. Most laboratory tests are aimed at determining the erosion rate of soils tested under controlled flow conditions. Laboratory tests on intact rock or rock masses are more challenging than those on soils, for the following reasons: (1) low erosion rate, (2) difficulty of obtaining reproducible data and (3) the scale effect. As a result, there are not much available data resulting from these tests on rock erosion, especially on the plucking behavior of rock masses.

A jet flow passing a spillway, or an overflow dam, often generates a scour hole in the plunge pool. Estimation of the scour-hole's potential depth is often an important concern for dam designs. Many empirical approaches have been proposed for estimating the ultimate depth of a scour hole in a granular riverbed. These approaches usually contain

* Corresponding author at: Department of Civil Engineering, National Chiao Tung University, 1001, University Road, Hsinchu 30010, Taiwan. Tel.: +886 3 5731931; fax: +886 3 5716257.
E-mail address: ywpan@mail.nctu.edu.tw (Y.-W. Pan).

0013-7952/$ – see front matter
http://dx.doi.org/10.1016/j.enggeo.2013.12.008

parameters (including the elevation drop, tail-water depth, maximum discharge and mean grain size) calibrated through a set of observed data (e.g., Martins, 1973; Mason and Arumugam, 1985).

Apart from these empirical approaches, some semi-empirical approaches were based on simplified principles of energy and/or momentum conservation and riverbed characteristics, with certain empirical correlations (e.g., Spurr, 1985; Akhmedov, 1988; Fahlbusch, 1994; Liu, 2005). Other approaches compare the stream power of water flow with the erodibility of the riverbed's geo-material to determine the maximum scouring depth (Annandale, 2005).

Noting that plucking is often responsible for the development of a scour hole on jointed rock masses, Bollaert (2002) proposed using the intensity of pressure fluctuations to evaluate the uplift displacement of the rock block, based on a dynamic impulsion concept. If the maximum uplift displacement reaches a critical ratio to the rock block's height, the block can escape, resulting in plucking. When the tail water becomes deeper, the intensity of the pressure fluctuations gradually declines. Eventually, there is a depth limit where plucking is no longer possible; ultimately, this limit is the scour-hole's depth.

Initially, if the discontinuities surrounding a rock block are not fully extended, the pressure fluctuations must first break all of the rock bridges before the block can be lifted. Bollaert (2002) employed a fatigue concept and attempted to model the crack propagation of a joint using basic fracture mechanics. He suggested comparing the stress intensity factor that corresponds to the maximum water pressure acting on the joint's end, with the fracture's toughness. If pressure fluctuations cannot cause fracture propagation in a single loading cycle, he proposed estimating the number of loading cycles required to extend the joint through an empirical relationship.

Robinson and Hanson (2001) studied the erosion of fractured rocks with physical tests, using a matrix of concrete blocks downstream of a controlled waterfall. Their results showed that the potential for block matrix failure depended on the maximum discharge, the waterfall's height, as well as the block's size and joint orientation. The pressure below the block matrix was measured; they pointed out that pressure variations on a block matrix were essential for the dislodgement of rock blocks and for plucking to cause erosion.

Several researchers conducted laboratory tests on models to investigate the induced pressure oscillation on a surface block due to jet flow (e.g., Castillo, 1989; Ervine et al., 1997). The pressures on the top (and sometimes the bottom) of the model block were measured and analyzed. Pressure fluctuations are often characterized by the non-dimensional mean dynamic pressure coefficient C_p and the non-dimensional root-mean-square (RMS) dynamic pressure coefficient C_p'. Coefficient C_p is the mean dynamic pressure head ratio to $\frac{V_j^2}{2g}$. The coefficient C_p' describes the intensity of the fluctuating dynamic pressure, and is defined by the following equation:

$$C_p' = \frac{(RMS/\gamma_w)}{\frac{V_j^2}{2g}} \tag{1}$$

where *RMS* is the root mean square of fluctuating dynamic pressure, and γ_w is the unit weight of water. The term $\frac{V_j^2}{2g}$ stands for the jet flow's kinetic energy with velocity V_j, and the symbol g represents the gravitational acceleration.

In general, coefficient C_p remains approximately unchanged for low tail-water depths (the limit is approximately 5) and decreases with an increase in the $\frac{Y}{D_j}$ when $\frac{Y}{D_j}$ is beyond the limit. Symbol Y represents the tail-water depth, and D_j denotes the jet flow's density. The coefficient C_p', increases with the increase in $\frac{Y}{D_j}$ and reaches its peak value at a critical $\frac{Y}{D_j}$ ratio (usually 5 to 7). For depth ratio $\frac{Y}{D_j}$ to be larger than the critical ratio, the C_p' declines when the $\frac{Y}{D_j}$ increases. The time history for pressure fluctuations from the jet flow is always irregular in nature, and its extreme amplitude can be a few times higher than the RMS (Bollaert, 2002). However, the time that is influenced by the extreme amplitude is extremely short.

Bollaert and Schleiss (2003) also conducted laboratory tests using a collection of metal plates fixed to the base of a water tank to imitate an artificial joint under a powerful jet flow. The purpose of this setup was to examine the pressure variations on the top and bottom of a riverbed's surface rock block due to the jet flow. Pore pressures on the top and bottom of the artificial joint were measured continuously throughout the test. Bollaert and Schleiss (2005) observed that the dominant frequency of pressure fluctuations at the joint's bottom is close to the fluid-joint system's fundamental resonance period, which depends on both the air-trapped water wave's velocity and the fracture's geometry. Because of the resonance, it is possible that the pressure is greater at the base of the block than at the top.

If the unbalanced instantaneous pressures acting on the top and bottom are able to overcome the buoyant weight and the joint resistances, the rock block can be lifted and displaced under pressure fluctuations. A power spectrum analysis of the measured pressure fluctuations shows that their frequency range is within 2 Hz and 500 Hz, and that the energy magnitude declines quickly with the increase in the frequency of pressure fluctuations (Bollaert and Schleiss, 2003). For example, the amplitude of a power spectrum corresponding to 100 Hz is two orders less than one that corresponds to 2 Hz.

Bollaert and Schleiss (2005) further evaluated the net force acting on a rock block with a width of x_b and height of z_b. The acting forces included the uplift, due to the jet pressure, the effective weight $(\gamma_s - \gamma_w) \cdot {x_b}^2 \cdot z_b$ and joint resistance F_{sh}. The terms γ_s and γ_w are the saturated unit weights for the rock and water, respectively. Uplift height h_{up}, from the resultant force, is derived from the following concept for dynamic impulsion:

$$h_{up} = \left[2\frac{(x_b + 2z_b)}{c}\right]^2 \cdot \frac{1}{2g \cdot {x_b}^4 \cdot {z_b}^2 \cdot {\gamma_s}^2} \times \left[C_I \cdot \gamma_w \cdot \frac{{V_j}^2}{2g} \cdot {x_b}^2 - (\gamma_s - \gamma_w) \cdot {x_b}^2 \cdot z_b - F_{sh}\right]^2 \tag{2}$$

where the term, $C_I \cdot \gamma_w \cdot \frac{{V_j}^2}{2g} \cdot {x_b}^2$, in the square bracket, stands for the magnitude of the uplift force acting on the rock block due to jet pressure. The uplift force is dependent on the jet flow's velocity V_j, jet flow thickness D_j and tail water depth Y. In Eq. (1), c is the water wave's velocity depending on the trapped air content.

Coefficient C_I in Eq. (2) denotes the dynamic impulsion coefficient. By compiling experimental data, Bollaert and Schleiss (2005) looked into the relationship between C_I and $\frac{Y}{D_j}$; by regression, they proposed an empirical parabolic function to express the relationship between C_I and $\frac{Y}{D_j}$. The coefficient C_I monotonically decreases with the increasing $\frac{Y}{D_j}$.

Bollaert and Schleiss (2005) suggested that the rock block's plucking potential could be evaluated by examining the $\frac{h_{up}}{z_b}$, and ascertained that the block could escape when the $\frac{h_{up}}{z_b}$ was greater than a critical ratio of 0.5. The jet-flow's velocity, when passing a spillway or an overflow dam differs with various floods, especially in the case of an overflow dam. The above approach uses the dynamic impulsion concept, and accounts for the largest flood that corresponded with a long returning period. The scour hole's maximum depth was determined by checking whether or not the $\frac{h_{up}}{z_b}$ was greater than 0.5 for the maximum discharge during the designated flood.

In principle, Bollaert–Schleiss's approach ignores the possible accumulation of smaller irreversible uplift displacements subjected to a lower intensity of pressure fluctuations corresponding to a shorter returning period. The question may be raised: Is it possible for the

smaller uplift displacement in an individual pressure fluctuation cycle to be cumulative and gradually lead to plucking? The following context will show that in spite of the fact that a discharge may not cause the ratio of $\frac{h_{up}}{z_b}$ to exceed the critical ratio in a single pressure cycle, it is still possible for the uplift displacement to be irreversible and cumulative, and to eventually cause plucking. To date, there has been little attempt to model the progressive incision of rock masses, through plucking, during a flood. A possible safety concern, for a spillway or a weir, is the growth of a scour hole during its life cycle.

This study first employs particle-flow simulations to model the progressive failure of rock bridges on a rock block's bottom plane when subjected to pressure fluctuations. It demonstrates how cumulative damage to rock bridges can gradually cause a weak plane to become fully persistent. This is followed up by a presentation of the fundamental mechanics and kinetics of a rock block subjected to pressure fluctuations from a jet flow. A parametric study is provided to explore the principal factors. Furthermore, an example demonstrates the applicability of the proposed approach on predicting the potential depth of scour hole.

2. Progressive failure of rock bridges subjected to pressure fluctuations

A surface rock block is usually made up of a base and several lateral discontinuities. Some of these discontinuities may contain rock bridges that are not fully persistent. With the presence of rock bridges, a surface rock block is initially constrained, and not free to uplift when subjected to pressure fluctuations. However, the repetitive action of pressure fluctuations has the potential to gradually remove the rock bridges. This phenomenon is demonstrated through numerical simulations using PFC^{3D} computer software that applies a discrete element method (DEM) to model the inter-granular reaction and the displacement of a collection of granular systems. This method employed by PFC^{3D} belongs to one class of the general discrete element methods, which may include the explicit DEM method and the implicit method of discontinuous deformation analysis (Jing and Stephansson, 2007).

By using PFC^{3D}, it is possible to model the gradual development of internal damage in a rock by tracing the successive bonding failure between adjacent particles. In PFC^{3D}, a bundle of inseparable balls (particles) can be glued together to form a "clump". A set of clumps can model the rock blocks in a jointed rock mass (Mas Ivars et al., 2011). A smooth joint is placed between any pair of neighboring clumps to model the mechanical behavior of the discontinuity between a pair of rock blocks. When using a smooth joint, the size of particles does not substantially affect the joints' apparent mechanical properties.

Even if a weak plane with rock bridges is not persistent at the beginning, a progressive loss of rock bridges may occur, along with a cumulative bond failure when repeated loadings are large enough. The loss of rock bridges is likely to start with some smaller disks, which may have been over-stressed, earlier. The remaining rock bridges can yield one by one and eventually lead to a total loss. Once all the rock bridges have been broken, the weak plane becomes fully persistent.

A series of simulations were conducted to qualitatively demonstrate the effects of repeated loadings on a weak base plane extension that originally had rock bridges. Fig. 1 illustrates the model of the simulations. Fig. 1(a) shows the assemblage of balls, the boundary walls and the applied loading condition. The sizes of balls are uniformly distributed within 15 mm and 25 mm. The shear resistance between any wall and its neighboring balls is ignored by setting the frictional coefficient to zero. The assemblage of balls is divided into two clumps; the repeated loading as a sinusoidal function of time is applied at the center of clump 1. Clump 2 is not allowed to move and is modeled as the underneath rock block. Fig. 1(b) displays the side view of the model showing the position of the smooth joint. The scenario considers the base plane of a rock block, measuring 0.7 m by 0.7 m by 0.5 m, as a bedding plane containing many rock bridges. Fig. 1(c) shows the distribution of contacts on the smooth joint; the effect of the rock bridges on the base discontinuity is modeled by including hundreds of contacts of various sizes. The strength of the contact bond on the smooth joint follows the Mohr–Coulomb criterion with frictional angle 30°. Two sets of smooth-joint bond strengths (for both tensile strength and cohesion) are assumed: 3 MPa for the case of virtual rock A, and 1 MPa for the

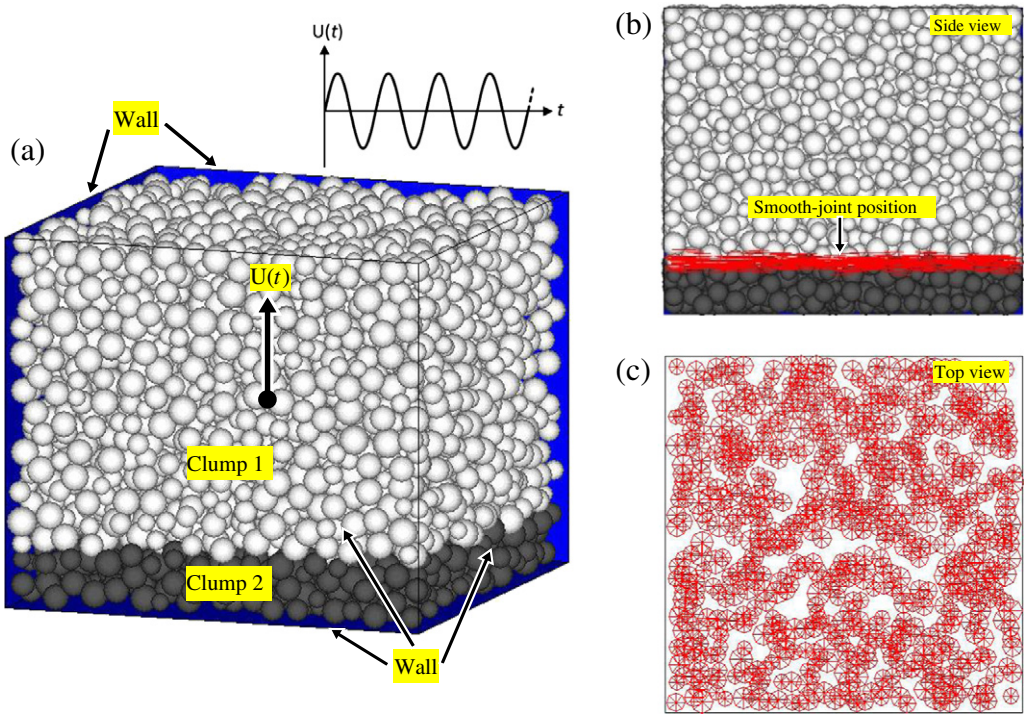

Fig. 1. Schematic illustration of the simulations using PFC^{3D}: (a) the model of particle assemblage and the applied loading; (b) the side view of the model; (c) the contacts on the smooth joint.

case of virtual rock B. Table 1 lists the input microscopic parameters in the PFC^{3D} simulations. Since the repeated loading acts along the normal direction of the discontinuity, the contact bonds can only fail in tension. Various levels of pressure fluctuations are applied to the rock block. The fluctuations of the different pressures are idealized as a sinusoidal wave with a 10 Hz frequency.

Two virtual blocks (A and B) with different pullout strengths were modeled. The ultimate strength for pulling out each virtual block directly represents the maximum resistance of the base discontinuity when subjected to a monotonically increasing load. This strength is hereafter defined as the "pull-out strength". As the intensity of pressure fluctuations p decreases, the number of cycles required to cause the weak base plane to fail increases. When the level of the pressure fluctuation is too small, a weak plane will not be damaged at all by stress cycles. Fig. 2 shows two curves, each compiling the simulated results of the number of load cycles required to destroy the weak plane through pressure fluctuations.

From the numerical simulation: the pull-out strength for virtual block A is 2 MPa, the pull-out strength for block B is 1.1 MPa. The difference in their pull-out strength is a result of their different smooth-joint bond strengths. It is possible for less intense pressure fluctuations to break the rock bridges on the weak plane when subjected to many cycles of repeated loading. For example, only two cycles with an intensity of 1.5 MPa were able to break all the rock bridges on block A. Many more cycles are required to pull out a specimen, if the pressure fluctuation's intensity is approximately 1.1 MPa. If the pressure intensity is lower than a certain threshold level, the rock block can never be pulled out, no matter how many pressure fluctuation cycles it endures.

Fig. 3 traces the ratio of bonding failure (to be denoted as "damage ratio" in Figure 2) at all the original contacts for the case with the pullout strength of 1.1 MPa. The damage ratio is defined by the number of the failed contact bonds divided by the total number of contact bonds on the weak plane (which is modeled by a smooth joint). The three curves in Fig. 2 show the damage ratio versus the number of loading cycles for three different intensities of pressure fluctuation p. In the model, the area for each rock bridge (represented by a contact) differs. The bonding at the smallest rock bridge tends to fail first because of its relative weakness; this tendency is supported by the simulated data (but not shown herein).

Once certain rock bridges lose their bonding, the resulting stress redistribution will cause a loading increase on the remaining undamaged rock bridges. As a result, the total pullout resistance gradually decreases. If p is close to the pullout strength, the damage ratio may quickly approach 100% after just a couple of cycles. When $p =$ 600 kPa, nearly 80% of the contact bonds has already failed at the end of the first cycle; no intact contact bond can survive after the second loading cycles. For a relative low intensity of pressure fluctuation (e.g., $p = 327$ kPa), only a small portion of the contact bonds fail in the first loading cycles; further loading cycles are required to remove the remaining bonds. Since fewer and fewer contact bonds are intact, the remaining contacts have to share higher contact force, and more likely to fail in successive loading cycles. Initially, the damage ratio builds up slowly, but will quickly accelerate when approaching the final stage. As a result, the curve gets steeper as the loading cycles increase.

Table 1
Input parameters for the simulations using PFC^{3D}.

Name	Value	Description
Density	2650 [kg/m^3]	Density
rlo	0.015 [m]	Minimum ball radius
rhi	0.025 [m]	Maximum ball radius
b_kn	5.0×10^6 [N/m]	Ball normal stiffness
b_ks	2.0×10^6 [N/m]	Ball shear stiffness
w_kn	5.0×10^6 [N/m]	Wall normal stiffness
w_ks	0 [N/m]	Wall shear stiffness
sj_kn	4.0×10^9 [Pa/m]	Smooth-joint normal stiffness per unit area
sj_ks	1.6×10^9 [Pa/m]	Smooth-joint shear stiffness per unit area
sj_fric	0.577	Smooth-joint frictional coefficient
sj_bns	3.0×10^6 & 1.0×10^6 [Pa]	Smooth-joint bond tensile strength
sj_bcoh	3.0×10^6 & 1.0×10^6 [Pa]	Smooth-joint bond cohesion

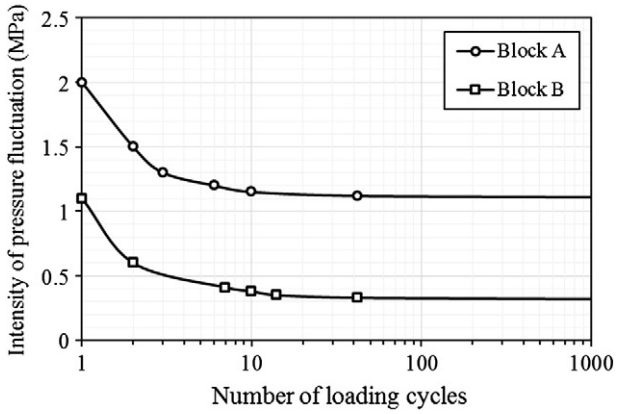

Fig. 2. Number of loading cycles required to open the weak plane by pressure fluctuation.

When all the rock bridges on a discontinuity become disconnected, the weak plane becomes fully persistent. It should be noted that this study only attempts to demonstrate this phenomenon qualitatively. A quantitative modeling on this subject requires more detailed and numerous simulations, which are beyond the scope of the present work.

The rock block cannot rise as long as the pressure fluctuations cannot overcome the rock bridges' bonding strength. Before the rock bridges are completely destroyed, the rock block cannot be lifted. If the pressure fluctuations' intensity is not vigorous enough, the base discontinuity remains undamaged and the cumulative uplift displacement cannot take place at all. Only when a pressure fluctuation is large enough to break the rock-bridge bonding, there is a chance for the accumulation of uplift displacement. When rock bridges are present, the rock block's uplifted motion is more restrictive, and the plucking action can be hindered or delayed.

3. The mechanics of a rock block subjected to pressure fluctuations

Fig. 4 is the schematic illustrations showing the conceptual model, and describing the mechanics of a rock block subjected to oscillated pressure, for the following formulations. The time dependent uplift force U, arising from the difference of pressures on the block's top, p_{top} and on the bottom, p_{bottom} (as illustrated in Figure 4(a)), may contribute to the uplifting action on a surface block. For simplification, this study modeled the fluctuating pressures on the top and bottom as a sinusoidal function. Depending on the different oscillated pressure phases on

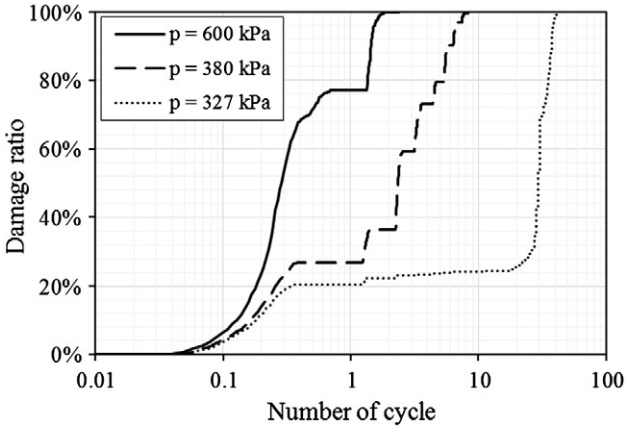

Fig. 3. Ratio of bonding failure against number of loading cycles.

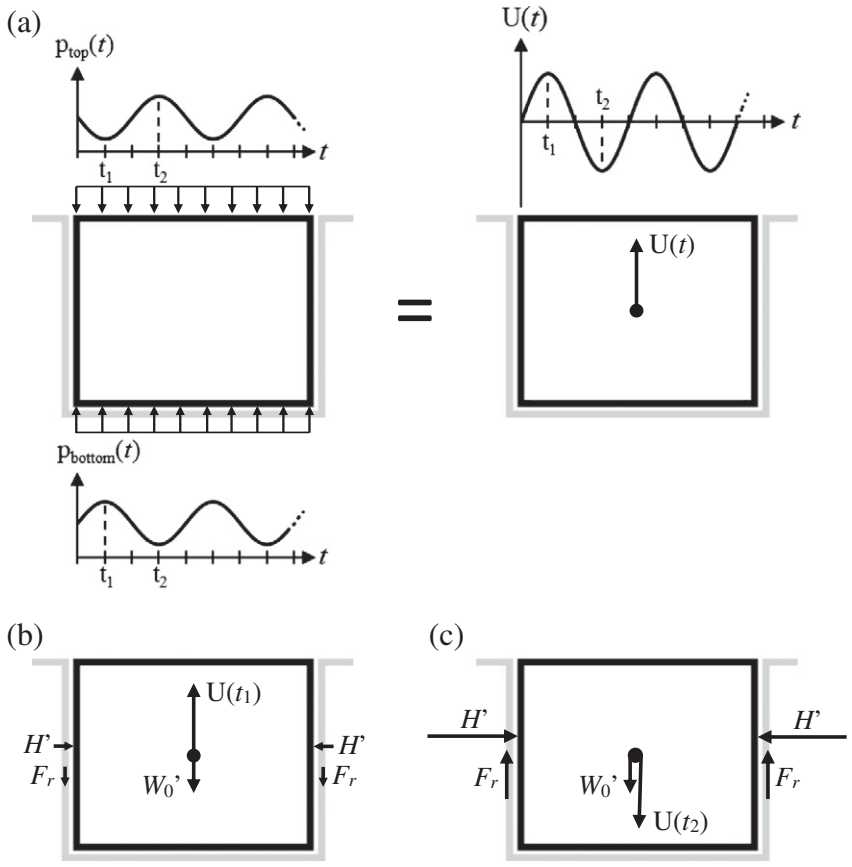

Fig. 4. Schematic illustrations for the mechanics of a rock block subjected to oscillated pressure: (a) the oscillated pressures and the equivalent uplift force *U(t)* acting on the rock block; (b) the forces acting on the rock block when *U* is upwards; (c) the forces acting on the rock block when *U* is downwards.

the block's top and bottom, *U* can be obtained from the pressure head difference as follows:

$$\Delta h = \alpha \cdot C_p^{'} \cdot \gamma_w \left(\frac{V_j^{\,2}}{2g}\right) \cdot \sin\omega t. \tag{3}$$

Therefore, the uplift force is $U = \gamma_w \cdot \Delta h \cdot A_1$, where A_1 is the top/bottom area. The uplift force *U* is positive when acting upwards.

Phase coefficient α accounts for the phase difference: $0 \le \alpha \le 2$. The phase coefficient is zero when the oscillated pressures on the top and bottom are in phase; but α is 2 when the oscillated pressure on the top and bottom has a phase difference of half a cycle. In the following context, it is assumed that the distribution of α is uniform; only its average value is considered (i.e. assuming $\alpha = 1.0$).

As long as the net uplift force on a rock block does not exceed the block's buoyant weigh $W_0{}'$, plucking will not take place. The net uplift force on a rock block is $U - W_0{}'$. When it is positive, the block can be lifted upwards.

The friction resistance on the lateral joints is mobilized with the upward displacement if the effective horizontal stress is compressive. In a steady condition, the average effective horizontal stress on a vertical joint can be expressed as the following equation:

$$\sigma_h^{'} = K_0 \cdot \gamma^{'} \cdot z. \tag{4}$$

In which γ' is the submerged unit weight, z is the average depth of the rock block and K_0 is the coefficient of the lateral stress at rest. Near the surface, K_0 is often close to, even larger than, 1.0.

The ultimate shear resistance force F_r can be estimated by the following equation:

$$F_r = \mu \cdot K_0 \cdot \gamma^{'} \cdot z_b{}^2 \cdot (x_b + y_b) \tag{5}$$

where μ is the frictional coefficient, and x_b, y_b and z_b are the rock block's size in x-, y- and z-directions, respectively. Eq. (5) is valid only when the pressure fluctuations on the top and base of a surface rock block are equal and in phase.

If the fluctuated pressures are not equal, or out of phase, there exists an instantaneous hydraulic gradient $\frac{\Delta h}{\Delta z}$ between the top and base of the rock block. In that situation, Eq. (4) should be corrected for the pressure head gradient. Then, the instantaneous effective vertical stress is time dependent.

For an upward gradient, the horizontal effective stress is expressed as follows.

$$\sigma_h^{'} = K_0 \cdot \left(\gamma' - \frac{\Delta h}{\Delta z} \cdot \gamma_w\right) \cdot z. \tag{6}$$

For a downward gradient, the horizontal effective stress is expressed as follow.

$$\sigma_h^{'} = K_0 \cdot \left(\gamma' + \frac{\Delta h}{\Delta z} \cdot \gamma_w\right) \cdot z. \tag{7}$$

The effective normal force on the lateral joints is $H' = K_0 \cdot W'$, where $W' = W_0{}' - U$ stands for the time-dependent effective weight of the rock block, and W' and $W_0{}'$ are positive for the downward direction.

It is impossible for plucking to occur if W' remains positive during pressure fluctuations. The necessary condition for plucking is that the hydraulic gradient is $\frac{\Delta h}{\Delta z} > \frac{\gamma_w}{\gamma'}$. However, this condition is insufficient to trigger plucking. This will be discussed further.

When the pressure at the bottom is greater than at the top, the vertical effective stress is lowered because of the hydraulic gradient (as illustrated in Figure 4(b)). It should be noted that the friction resistance on the lateral joint does not exist whenever σ_h' is no longer compressive, which happens when $W' < 0$. Consequently, the ultimate frictional resistance from the lateral friction can be expressed as follows:

$$F_r = \mu \cdot K_0 \cdot \frac{\max[W', 0]}{2} \cdot A_2 \tag{8}$$

where A_2 stands for the total area of the lateral side faces. For a rectangular rock block, side area A_2 is simply $2(x_b + y_b) \cdot z_b$. The ultimate frictional resistance can be expressed as follows:

$$F_r = \mu \cdot K_0 \cdot \max\left[\left(\gamma' - \left(\frac{\alpha \cdot C_p' \cdot \left(\frac{V_j^2}{2g}\right)}{z_b}\right) \cdot \gamma_w\right), 0\right] \cdot z_b^2 \cdot (x_b + y_b). \tag{9}$$

The minimum allowable frictional resistance is zero, i.e. $F_{r,\min} = 0$.

When the pressure at the top is greater than at the base, the effective stress is raised so that the ultimate shear resistance force can increase substantially (as illustrated in Figure 4(c)):

$$F_r = \mu \cdot K_0 \cdot \frac{W'}{2} \cdot A_2. \tag{10}$$

Thus,

$$F_r = \mu \cdot K_0 \cdot \left(\gamma' + \gamma_w \frac{\Delta h}{z_b}\right) \cdot z_b^2 \cdot (x_b + y_b). \tag{11}$$

However, the ultimate shear resistance can never exceed the resultant forces of the effective weight and the total uplift force when the sliding velocity is in the same direction as W'. This constraint can be expressed as $F_{r,\max} \le |W'|$.

R denotes the resultant of W' and F_r; and $V_b = x_b \cdot y_b \cdot z_b$ denotes the rock block's volume. The maximum possible upward resultant is $R_\uparrow = \left(\frac{\Delta h}{z_b} \cdot \gamma_w - \gamma'\right) \cdot V_b$; it is only positive when $\frac{\Delta h}{z_b} > \frac{\gamma'}{\gamma_w}$. For this condition there is no frictional resistance, and the frictional coefficient has no effect on the resultant. It is noted that the term $\frac{\gamma'}{\gamma_w}$ is approximately constant for most rocks.

By assuming $x_b = y_b$, the maximum downward resultant is as follows:

$$R_\downarrow = \max\left\{\left[\left(\gamma' + \frac{\Delta h}{z_b} \cdot \gamma_w\right)\left(1 - 2\mu \cdot K_0 \cdot \left(\frac{z_b}{x_b}\right)\right) \cdot V_b\right], 0\right\}. \tag{12}$$

The non-dimensional parameter $\mu^* = 2\mu \cdot K_0 \cdot \left(\frac{z_b}{x_b}\right)$ appears to be an effective index for the consideration of the frictional resistance factor. As noted from the equation above, the maximum downward resultant $R_\downarrow$ remains positive as long as $\mu^* < 1$. Under this condition, the rock block can be displaced downward because the ultimate frictional resistance is not large enough to overcome the downward forces. Once $\mu^* > 1$, $R_\downarrow$ will quickly approach zero, and the rock block's downward movement will be stopped before the friction resistance reaches the ultimate resistance. A higher frictional resistance tends to hinder the block's downward movement more effectively while $U < 0$ (when the pressure on the block top is greater than that on the bottom), and helps to cumulate the upward displacement in a full pressure fluctuation cycle.

It is recognized that some assumptions made while deriving the above formulation do not exactly duplicate the real conditions. For example: the uplift force acting on a rock block is assumed to follow Eq. (3) in the form of sinusoidal function of time with $\alpha = 1.0$. This of course may differ from the expected irregularly oscillated pressure under a jet flow. Nevertheless, the simplification of the irregular oscillated uplift force to an equivalent sinusoidal function is considered to be an acceptable simplified approach for the evaluation of cumulative uplift displacement. Besides, the above formulation has assumed that each rock block is cubic with vertical lateral joints and with horizontal top and bottom faces. Again, these assumptions may not be exactly in accordance with the reality. Yet, it is possible to approximate a rock block to a cubic block with the same projected area on three mutually orthogonal planes to obtain the equivalent sizes of x_b, y_b and z_b.

4. Response of a rock block subjected to pressure fluctuations

The inertia acceleration of a rock block with mass m_b when subjected to resultant R, is $a = {}^{R}/_{m_b}$. Since resultant R is a periodic function, the inertia acceleration is also periodic. The acceleration integration yields the velocity. The displacement of the block can be obtained through successive integrations of velocity.

The block's movement can be repeated cycle by cycle. The first case occurs when ultimate F_r is not large enough to overcome the downward W' so the block descends. However, the cumulative uplift displacement is not allowed to be negative since the block cannot move beyond its original position. When the block returns to its original position and the result is downward, the downward velocity and displacement reduces to zero. The other case occurs when the ultimate F_r exceeds the downward W'. Then the zero resultant force will soon reach and stop the rock block's downward movement very quickly. In both cases, the rock movement's downward velocity has to return to zero at the end of every pressure fluctuation's cycle.

The rock block's velocity must also be a periodic function. However, the displacement may or may not be periodic when there is a net gain of upward displacement within just one cycle. The upward displacement can accumulate cycle by cycle. With a specific pressure fluctuation frequency, one can obtain the uplift speed of a rock block subjected to numerous load cycles, by repeating it over and over within a time unit. On the other hand, if there is no net upward displacement within one loading cycle, plucking is impossible no matter how long the pressure fluctuation lasts.

Fig. 5 illustrates three scenarios of a rock block's response in a single pressure fluctuation cycle: Case 1 has a permanent uplift displacement without any return, Case 2 has a permanent uplift displacement with partial return, and Case 3 does not have a permanent uplift displacement. The abscissa is the non-dimensional time, t/T, in which T is the period of pressure fluctuation. All the results in Fig. 4 were obtained by applying the theory presented in the last section. In both cases, the prescribed conditions are as follows:

1. The rock block's dimensions are $x_b = y_b = z_b = 0.5$ m;
2. The friction coefficients for these two cases are 0.5, 0.4 and 0.3, respectively;
3. The coefficient for lateral pressure K_0 is 1.0;
4. The intensity of pressure-head fluctuation Δh is 5 m.

Therefore, the normalized parameters μ^* for each of the cases are 1.0, 0.8 and 0.6, respectively and the pressure-head gradient is 10.0. In Fig. 5, the first column is for Case 1, the second column for Case 2 and the third column for Case 3.

Fig. 5(a)–(c) shows the non-dimensional net uplift force due to pressure gradient $U^* = U/W_0'$ and effective weight $W'^* = W'/W_0'$ for each case during a pressure fluctuation cycle. All of the time-

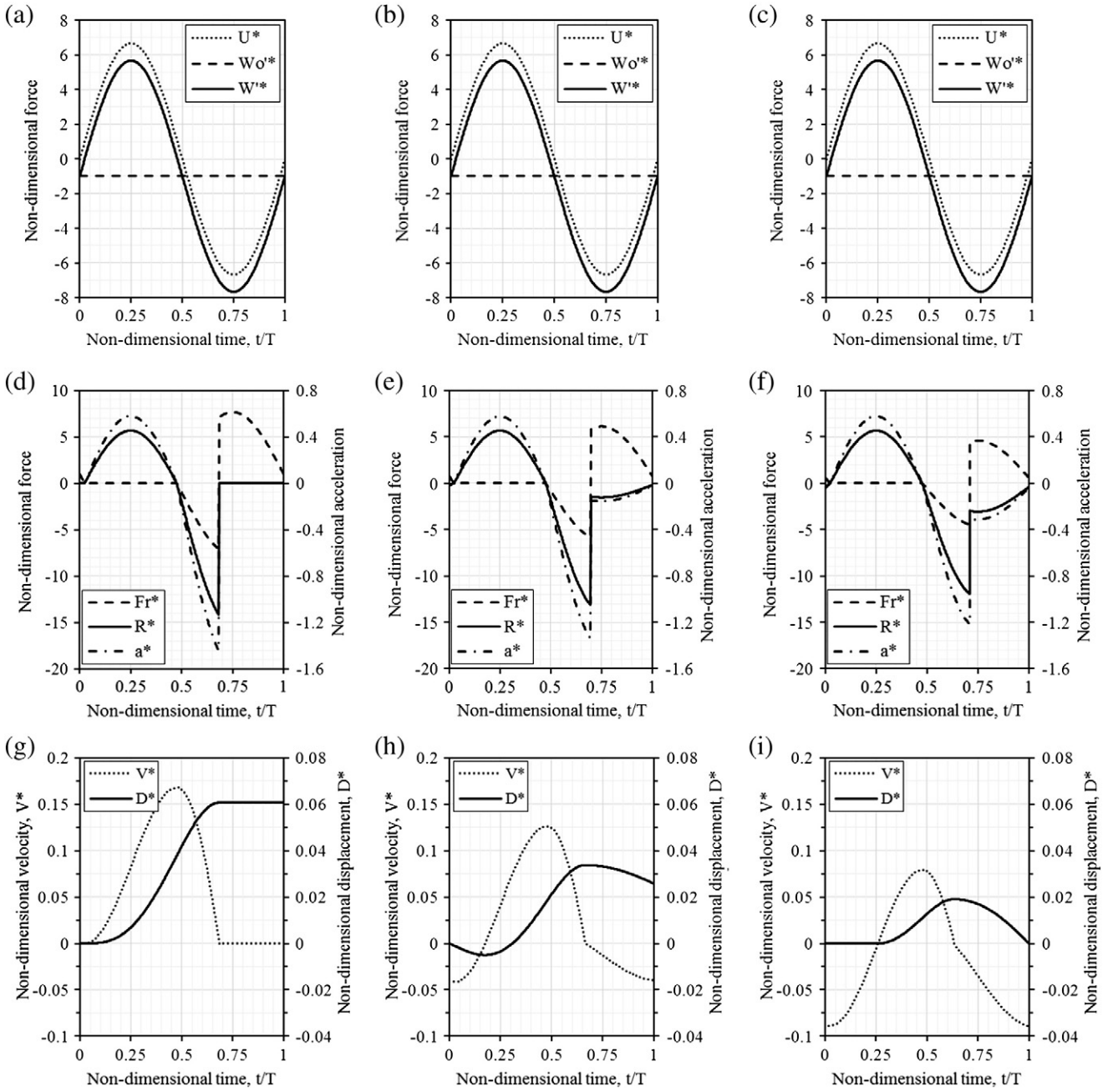

Fig. 5. The acting forces and response of a rock block within a single cycle of pressure fluctuation.

dependent force terms are identical for both cases. Fig. 5(d)–(f) shows the non-dimensional frictional resistance $F_r^* = F_r/W_0'$ and resultant force $R^* = R/W_0'$ in a cycle. The sign for each force is positive when the direction is upwards. The star by each term indicates that it is non-dimensional. In addition to the force terms, Fig. 5(d)–(f) also shows the rock block's non-dimensional inertia acceleration $a^* = a/g$.

Fig. 5(a)–(f) shows the variations and inter-relations of all the active forces. As shown in Fig. 5(a)–(c), U^* and W'^* are periodic functions. The rock block's time-dependent effective weight W' varies along with U^*: as U^* increases, the effective weight W' decreases correspondingly, and vice versa.

The direction for frictional resistance F_r is always towards the opposite direction of the block's velocity; its ultimate resistance is proportional to W' when the effective horizontal force remains compressive. Fig. 5(d)–(f) also shows the variations of non-dimensional F_r. When the uplift force U is too high, the horizontal effective force can become non-compressive and the corresponding frictional resistance F_r disappears. However it recovers once U starts to descend, but later increases along with the rock block's downward movement, although it can never exceed the sum of all the other acting forces. Resultant R is zero as long as the frictional resistance can balance the other acting forces. The solid lines in Fig. 5(d)–(f) are the non-dimensional resultant force R^*, including W'^* and F_r^*.

If resultant R is not zero, there is a corresponding inertia acceleration where $a = {}^{R}/_{m_b}$. Fig. 5(g)–(i) shows the non-dimensional velocity $V* = \frac{V}{T \cdot g}$ and the block's displacement $D* = \frac{D}{T^2 \cdot g}$ in a cycle, in which T is the period of pressure fluctuation. Velocity V is obtained through integrating acceleration over time. Successive velocity integration produces displacement D. However, the downward velocity and displacement must be set at zero once the rock block returns to the base level (i.e. the original position of the block).

Comparing the three distinct cases, the rock block's response can be different for ultimate F_r, even if the intensity of pressure fluctuations and the rock-block dimensions remain unchanged. In Case 1, the ultimate F_r is large enough to fully stop the rock block's downward movement. Thus, no block's downward return can occur (Figure 5(g)). In Case 2, the upward displacement in the early part of the cycle is greater than any subsequent downward movements, so there is a net uplift displacement gain in a single cycle (Figure 5(h)). In Case 3, the ultimate F_r is not enough to balance the subsequent downward forces. The block can move all the way back down to its base level at the end of each loading cycle (Figure 5(i)). In each cycle, the uplift in the early part of the cycle is canceled out by the subsequent sinking. Therefore, if the net uplift displacement in one cycle is zero, then it is impossible to accumulate any uplift displacement in that cycle. The role of frictional resistance is not to resist the block's uplift, but rather to hinder its downward displacement.

It should be noted that non-dimensional D^*, in a pressure-fluctuation cycle, is not affected by the pressure fluctuation's frequency (f). The cumulative uplift velocity in unit time V_{up} can be obtained by $V_{up} = D \cdot f = D^* \cdot (T^2 \cdot g) \cdot f = D^* \cdot T \cdot g$ since $f = 1/T$. It appears that the cumulative uplift velocity in a time unit is proportional to the pressure fluctuation period. The higher the frequency, the lower V_{up} will be.

If the net uplift displacement D in one cycle is zero, then V_{up} is zero, whether or not D is zero depends on the capacity of ultimate F_r. The non-dimensional parameter μ^* is an effective index determining whether the ultimate frictional resistance capacity is sufficient for stopping the block's downward movement when the net pressure also goes down. In the case of $\mu^* > 1$, the block's downward movement can be ignored. The net uplift displacement in one single cycle exists as long as $\frac{\Delta h}{z_b} > \frac{\gamma'}{\gamma_w}$.

Fig. 6 displays the relationship of the non-dimensional uplift displacement D^* in a cycle against the pressure head gradient $\left(\frac{\Delta h}{z_b}\right)$ for various parameter combinations. D^* is the non-dimensional uplift displacement in a pressure-fluctuation cycle. The results for a variety of parameter combinations are compiled in Fig. 6. Table 2 lists the combinations of parameters and variables used for the generation of this figure. The parameter combinations are purposely divided into several groups with distinct values of the non-dimensional parameter μ^*. The pressure head gradient $\left(\frac{\Delta h}{z_b}\right)$ covers a wide range to examine the variation of D^* under various pressure head gradients. Since the mechanism of plucking is more likely for sub-meter rock blocks (Whipple et al., 2000), the sizes x_b and z_b were deliberately chosen so that the block volume is smaller than 1 cubic meter and the aspect ratio $\frac{z_b}{x_b}$ is equal to certain constants.

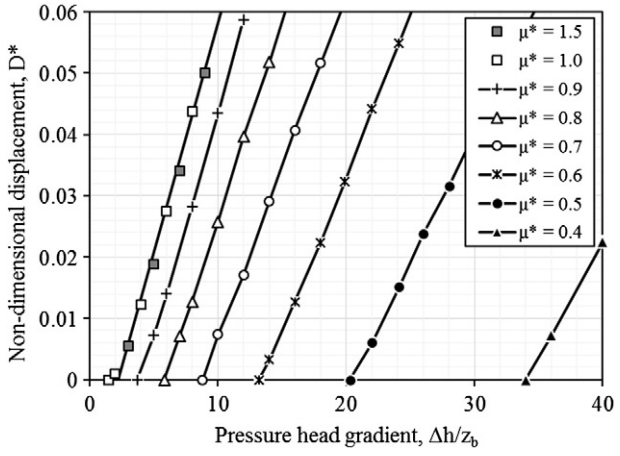

Fig. 6. The relations between D^* and $\frac{\Delta h}{z_b}$ for various μ^*.

The normalized displacement D^* is always zero when $\frac{\Delta h}{z_b} < \frac{\gamma'}{\gamma_w}$; in other words, the on-set $\frac{\Delta h}{z_b}$ for $D^* > 0$ is equal to $\frac{\gamma'}{\gamma_w} \cong 1.5$. As $\frac{\Delta h}{z_b} > \frac{\gamma'}{\gamma_w}$, the normalized displacement D^* increases with the increase in $\frac{\Delta h}{z_b}$. As long as $\mu^* \geq 1$, the relationships of D^* against $\frac{\Delta h}{z_b}$ for different μ^* remains approximately identical because the block is unable to move downwards at all.

In cases $\mu^* < 1$, the ultimate frictional resistance cannot match the downward resultant in the latter part of a pressure-fluctuation cycle, so the block moves downwards in response. However, the downward non-zero resultant in the latter part of the cycle does not guarantee that the block can move back to its original base position. A lower level of μ^* indicates a greater insufficiency of frictional resistance, resulting in a larger downward resultant R to bring the block back down to its base position. An intermediate level of μ^* corresponds to a situation where the block can only move halfway down, and does not return to its original base position.

For $\mu^* < 1$, the criterion $\frac{\Delta h}{z_b} > \frac{\gamma'}{\gamma_w}$ will not guarantee a net gain in the block uplift displacement. A higher pressure-head gradient is required to cause the block to move upwards in a cycle. The lower μ^* is, the higher the critical $\frac{\Delta h}{z_b}$ needs to be in order to lift the block. For example, the critical $\frac{\Delta h}{z_b}$ required for $\mu^* = 0.9$ is approximately 3.5, while the minimum $\frac{\Delta h}{z_b}$ required for $\mu^* = 0.7$ is nearly 9. If the $\frac{\Delta h}{z_b}$ is smaller than the critical value, the block returns to its base position at the end of each cycle, so that the net displacement for each cycle is always zero and there is no cumulative uplift displacement. In a case where $\frac{\Delta h}{z_b}$ is larger than the critical value, the block can never return to its original position. In each cycle, the early upward displacement is always larger than one in the latter part of the cycle. Consequently, each cycle has a net uplift displacement that generates a cumulative uplift displacement.

The presented formulation is intended to model the plucking response of a rock block subjected to jet flow, and is readily applicable for predicting the potential depth of a scour hole under the jet flow during a flood event. The principle of the model should also be effective for modeling the plucking of rock blocks on a natural river bed or river bank due to turbulent stream flow provided that the oscillated pressure acting on the superficial rock block is given. However, to the best knowledge of the authors, there is no empirical relation available for estimating the amplitude of oscillated pressure acting on a surface rock block due to violent stream flow. Yet, it is possible to estimate the amplitude of oscillated pressure from the measured results of physical model tests modeling the field conditions of the stream flow on top of the considered natural river bed. In that case, the presented formulation can be directly applied to the plucking evaluation of a natural river bed.

Alternatively, it is also possible to estimate the intensity of the quasi-steady lift force L on a surface rock block arisen from channel flow with a velocity $V_{channel}$. Reinius (1986) conducted physical model tests and compiled the non-dimensional quasi-steady uplift pressure C_{up}' on a protruding surface rock block with various geometry configuration; the value of C_{up}' depends on the aspect ratio and the joint orientation of rock blocks. By adopting C_{up}', the quasi-steady lift force L acting on a rock block, with an exposure area $A_{\exp}$, due to a channel flow with a velocity $V_{channel}$ can be estimated by the following equation:

$$L = C_{up}' \cdot \gamma_w \cdot \frac{V_{channel}^2}{2g} \cdot A_{\exp}. \tag{13}$$

As long as L can overcome the buoyant weigh W_0' of a surface rock block on river bed, plucking of this block can take place.

5. Application on the evaluation of potential scour-hole depth

The proposed model is applied to the case study of the scour hole in front of the toe of the *Yi-Xing* Dam on the *Da-Han* River, Taiwan, to

Table 2
The parameters used and the data in Fig. 6.

μ*	Volume (m^3)	x_b	z_b	Δh	$\frac{\Delta h}{z_b}$	D*	μ*	Volume (m^3)	x_b	z_b	Δh	$\frac{\Delta h}{z_b}$	D*
1.5	0.2	0.51	0.77	1.1	1.5	0	0.7	0.4	0.83	0.58	5.1	8.8	0
1.5	0.4	0.64	0.97	2.9	3	5.51E−03	0.7	0.2	0.66	0.46	4.6	10	7.36E−03
1.5	0.2	0.51	0.77	3.8	5	1.89E−02	0.7	0.4	0.83	0.58	7.0	12	1.70E−02
1.5	0.4	0.64	0.97	6.8	7	3.41E−02	0.7	0.2	0.66	0.46	6.5	14	2.91E−02
1.5	0.2	0.51	0.77	6.9	9	5.00E−02	0.7	0.4	0.83	0.58	9.3	16	4.07E−02
1.0	0.4	0.74	0.74	1.1	1.5	0	0.7	0.2	0.66	0.46	8.3	18	5.16E−02
1.0	0.2	0.58	0.59	1.2	2	9.02E−04	0.6	0.4	0.87	0.52	6.9	13.2	0
1.0	0.4	0.74	0.74	2.9	4	1.23E−02	0.6	0.2	0.69	0.42	5.8	14	3.26E−03
1.0	0.2	0.58	0.59	3.5	6	2.75E−02	0.6	0.4	0.87	0.52	8.4	16	1.27E−02
1.0	0.4	0.74	0.74	5.9	8	4.38E−02	0.6	0.2	0.69	0.42	7.5	18	2.24E−02
0.9	0.4	0.76	0.69	2.5	3.7	0	0.6	0.4	0.87	0.52	10.4	20	3.23E−02
0.9	0.2	0.61	0.55	2.7	5	7.27E−03	0.6	0.2	0.69	0.42	9.2	22	4.42E−02
0.9	0.4	0.76	0.69	4.1	6	1.40E−02	0.6	0.4	0.87	0.52	12.6	24	5.49E−02
0.9	0.2	0.61	0.55	4.4	8	2.82E−02	0.5	0.4	0.93	0.46	9.4	20.3	0
0.9	0.4	0.76	0.69	6.9	10	4.34E−02	0.5	0.2	0.74	0.37	8.1	22	6.06E−03
0.9	0.2	0.61	0.55	6.5	12	5.88E−02	0.5	0.4	0.93	0.46	11.2	24	1.52E−02
0.8	0.4	0.79	0.63	3.7	5.8	0	0.5	0.2	0.74	0.37	9.6	26	2.39E−02
0.8	0.2	0.63	0.50	3.5	7	7.08E−03	0.5	0.4	0.93	0.46	13.0	28	3.16E−02
0.8	0.4	0.79	0.63	5.1	8	1.27E−02	0.5	0.2	0.74	0.37	11.8	32	4.89E−02
0.8	0.2	0.63	0.50	5.0	10	2.58E−02	0.4	0.4	1.00	0.40	13.6	34	0
0.8	0.4	0.79	0.63	7.6	12	3.96E−02	0.4	0.2	0.79	0.32	11.4	36	7.21E−03
0.8	0.2	0.63	0.50	7.1	14	5.18E−02	0.4	0.4	1.00	0.40	16.0	40	2.25E−02

demonstrate its applicability. The *Yi-Xing* Dam is an overflow type of gravity dam completed in 1973. The outcrop in the dam site is the Miocene *Mu-San* Formation composed of heavily jointed sandstone. The unconfined compressive strength of the sandstone is approximately 80 MPa. The unit weight of the rock material is 25 kN/m^3. The outcrop strata contain three orthotropic sets of weak planes; rock blocks are formed by these three set of discontinuities. The estimated thickness of rock block z_b is within 0.5 m and 1 m, while the mean ratio of $\frac{z_b}{x_b}$ is approximately 0.5. The estimated frictional coefficient μ is 0.5 and K_0 is 1.0. As a result, the non-dimensional parameter μ^* is 0.5.

A cross-section survey of the scour hole was conducted in 2008. The intense scouring that occurred in front of the *Yi-Xing* Dam's toe formed a giant hole with a maximum depth exceeding 13 m. The outcrop contains heavily jointed rock masses in the dam site; blocky remnants are clearly observable in the downstream adjacent to the scour hole. Based on field observation, it is evident that the major erosive mechanism in the scour hole was caused by plucking, as a result of jet flow.

The hydrologic event that occurred during Typhoon *Aere* in 2004 was adopted for the demonstration. This typhoon brought a peak discharge of 7361 m^3/s to the *Yi-Xing* Dam; it is the maximum discharge since the dam was completed. This discharge corresponds approximately to the peak discharge of the 25-year return period Q_{25}. A series of hydraulic analyses for discharge corresponding to various return periods were conducted for the *Yi-Xing* Dam by the Water Resources Agency of Taiwan (WRA, 2010). The flow velocity V_i and the thickness D_i for various of flow passing the dam crest can be retrieved from this report. Denote V_j and D_j as the velocity and thickness, respectively of the jet flow while hitting the tail water. V_j can be calculated from V_i by taking the water-level drop and the energy conservation into account; D_j can be obtained simply by means of the continuous equation.

The discharge Q_{25} was adopted for evaluating the potential scour-hole depth using the proposed model. For Q_{25}: $V_i = 19$ m/s, $D_i = 2.6$ m, $V_j = 23$ m/s and $D_j = 2.1$ m. The elevations at the dam crest and at the surface of the tail water are 277 m and 271 m, respectively. Before the Dam's completion, the elevation at the riverbed in front of the dam's toe was 258 m. The elevation at the plunge base was 245 m in 2008. Fig. 7 is the schematic illustrations showing the elevations of the dam crest, the bed elevation, and the tail-water surface.

As the scour hole gets deeper, Y increases; as a result, $\frac{Y}{D_j}$ also increases. Fig. 8 shows a curve relating the non-dimensional RMS dynamic pressure coefficient C_p' to $\frac{Y}{D_j}$. The data were the experimental results by Castillo (1989) from experiments of jet flow through a rectangular opening. A regression curve is derived in the present work. For $\frac{Y}{D_j}$ larger than 5, C_p' decreases monotonically with increasing $\frac{Y}{D_j}$. No condition for $\frac{Y}{D_j}$ smaller than 5 can occur in the case of the *Yi-Xing* Dam. Given z_b and V_j, there is a one-to-one relationship between C_p' and $\frac{\Delta h}{z_b}$. Fig. 9 presents two curves of $\frac{Y}{D_j}$ against $\frac{\Delta h}{z_b}$ for z_b equal to 0.5 and 1.0, respectively; they overlap the curves, as those shown in Fig. 5. For $\mu^* = 0.5$, the critical pressure head gradient $\frac{\Delta h}{z_b}$ for a block to produce irreversible uplift translation in one cycle is approximately 20. The ratio $\frac{Y}{D_j}$ corresponding to $\frac{\Delta h}{z_b} = 20$ for $z_b = 0.5$ and $z_b = 1.0$ are approximately 10 and 14, respectively. The elevation at the plunge pool base in 1971 was 258 m, which was 13 m below the tail-water surface. Since D_j is 2.1 m, the depth of tail water Y is within 21.0 m and 29.4 m. Therefore, the estimated scour-hole depth is within 8.0 and 16.4 m; the range agrees with the surveyed data. This case study demonstrates the

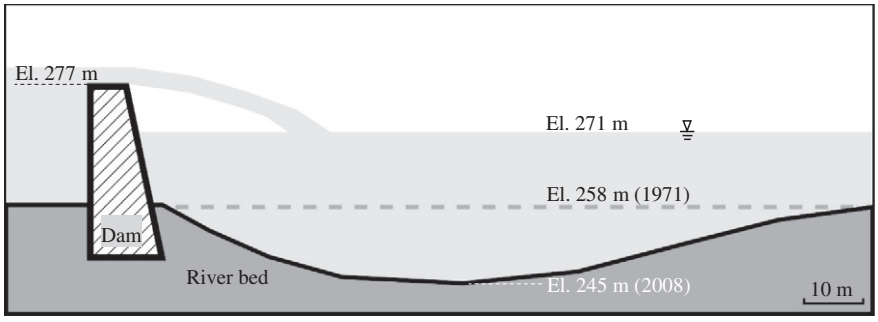

Fig. 7. Schematic illustration of the elevations of dam crest, river bed, and tail-water surface.

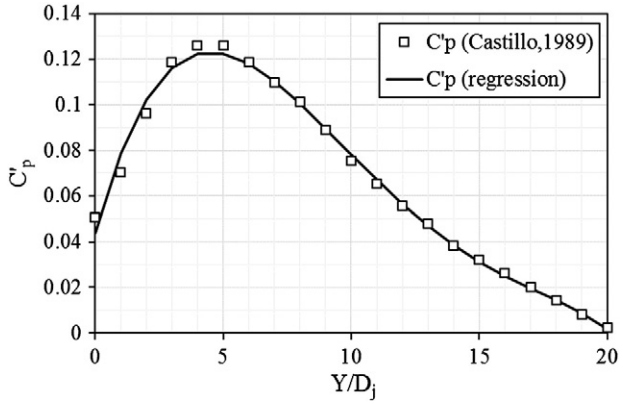

Fig. 8. The relation between C_p' and $\frac{Y}{D_j}$. Data retrieved from Castillo (1989).

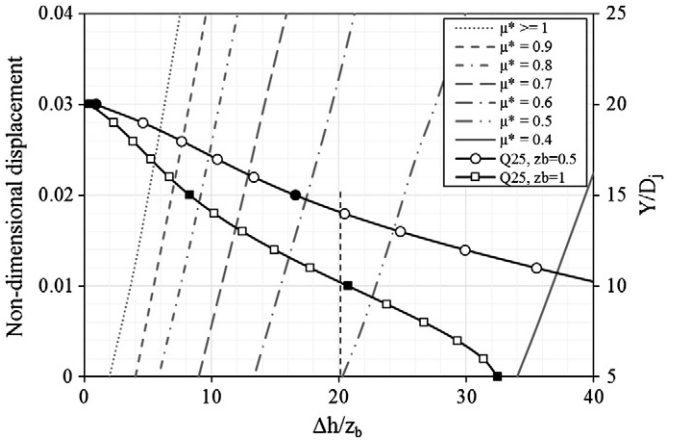

Fig. 9. The relations between $\frac{Y}{D_j}$ and $\frac{\Delta h}{z_b}$ for two block thicknesses together with the relations between D^* and $\frac{\Delta h}{z_b}$ for various μ^*.

applicability of the proposed approach for evaluating the potential depth of a scour hole due to plucking.

The result can further be compared with the Bollaert's method for calculating the maximum scour hole depths (Bollaert, 2002). Using the method of dynamic impulsion by means of Eq. (1) with the in situ parameters, the calculated h_{up}/z_b does not exceed 0.05. With the low ratio of h_{up}/z_b, intense scouring should not have occurred at all. It seems the result derived by dynamic impulsion fails to explain what has already happened in the13-m scour hole.

6. Concluding remarks

Plucking is often the dominant mechanism for a scour hole on a riverbed composed of heavily jointed rock masses subjected to pressure fluctuations (e.g., due to a jet flow). This paper explored the mechanics of a surface block's response when subjected to pressure fluctuations, and came to the following conclusions.

1. Results of a particle-flow simulation demonstrated that repeated pressure fluctuations are able to gradually remove the rock bridges in discontinuities if the pressure fluctuation's intensity is substantial enough. As a consequence, these weak planes become fully persistent.
2. After the discontinuities around a surface block become fully persistent, the block becomes free and its uplift response depends on the different pressures on the opposite (horizontal) faces and the frictional resistance of the lateral discontinuities.
3. This paper proposes a theoretical framework to model and explore the mechanics and response of a rock block subjected to a sinusoidal pressure fluctuation.
4. Pressure head gradient $\frac{\Delta h}{z_b}$ has to exceed the minimum level equal to $\frac{\gamma'}{\gamma_w}$ to drive a surface rock block upwards. A higher $\frac{\Delta h}{z_b}$ tends to result in a higher uplift rate when a non-zero uplift displacement is present.
5. The direction of pressure head gradients determines the effective stress, controlling the level of the lateral ultimate frictional resistance. When the pressure head gradient is upward, the frictional resistance is largely reduced, and vice versa.
6. The role of frictional resistance is not to resist the block uplift, but to hinder the return of the downward displacement. The non-dimensional parameter $\mu^* = 2\mu \cdot K_0 \cdot \left(\frac{z_b}{x_b}\right)$ is an effective index describing the capacity of the ultimate frictional resistance. As $\mu^* > 1$ and $\frac{\Delta h}{z_b} > \frac{\gamma'}{\gamma_w}$, the cumulation of uplift displacement can always take place. For a small μ^*, the block always returns to its original base level at the end of each cycle; uplift displacement and plucking is not possible.
7. The proposed model was applied to a case study of the scour hole in front of a dam's toe. The estimated depth of scour hole appears to agree with the measured data. The case study demonstrates the applicability of the proposed model in predicting the potential depth of scour hole due to plucking.

Acknowledgments

The work presented in this paper was made possible through the support of the National Science Council (Project no. 101-2625-M-009-012).

References

Akhmedov, T., 1988. Calculation of the depth of scour in rock downstream of a spillway. Int. Water Power Dam Constr. 40 (12).
Annandale, G., 1995. Erodibility. J. Hydraul. Res. 33 (4), 471–494.
Annandale, G., 2005. Scour Technology: Mechanics and Engineering Practice. McGraw-Hill Professional.
Bollaert, E., 2002. Transient Water Pressures in Joints and Formation of Rock Scour due to High-velocity Jet Impact. Ecole Polytechnique Fédérale de Lausanne.
Bollaert, E., Schleiss, A., 2003. Scour of rock due to the impact of plunging high velocity jets part II: experimental results of dynamic pressures at pool bottoms and in one- and two-dimensional closed end rock joints. J. Hydraul. Res. 41 (5), 465–480.
Bollaert, E.F., Schleiss, A.J., 2005. Physically based model for evaluation of rock scour due to high-velocity jet impact. J. Hydraul. Eng. 131 (3), 153–165.
Castillo, L., 1989. Metodología experimental y numérica para la caracterización del campo de presiones en los disipadores de energía hidráulica. (Tesis de Doctorado) Aplicación al vertido libre en presas bóveda.Universidad Politécnica de Cataluña, Barcelona.
Cook, K.L., Turowski, J.M., Hovius, N., 2013. A demonstration of the importance of bedload transport for fluvial bedrock erosion and knickpoint propagation. Earth Surf. Process. Landforms 38 (7), 683–695.
Ervine, D., Falvey, H., Withers, W., 1997. Pressure fluctuations on plunge pool floors. J. Hydraul. Res. 35 (2), 257–279.
Fahlbusch, F., 1994. Scour in rock river beds downstream of large dams. Int. J. Hydropower Dams 1 (4), 30–32.
Huang, M.-W., Pan, Y.-W., Liao, J.-J., 2013. A case of rapid rock riverbed incision in a coseismic uplift reach and its implications. Geomorphology 184, 98–110.
Jing, L., Stephansson, O., 2007. Fundamentals of Discrete Element Methods for Rock Engineering: Theory and Applications. Elsevier Science.
Liu, P., 2005. A new method for calculating depth of scour pit caused by overflow water jets. J. Hydraul. Res. 43 (6), 696–702.
Martins, R., 1973. Contribution to the knowledge on the scour action of free jets on rocky river beds. 11th Congress on Large Dams.: Madrid, pp. 799–814.
Mas Ivars, D., Pierce, M.E., Darcel, C., Reyes-Montes, J., Potyondy, D.O., Paul Young, R., Cundall, P.A., 2011. The synthetic rock mass approach for jointed rock mass modelling. Int. J. Rock Mech. Min. Sci. 48 (2), 219–244.
Mason, P.J., Arumugam, K., 1985. Free jet scour below dams and flip buckets. J. Hydraul. Eng. 111 (2), 220–235.
Reinius, E., 1986. Rock erosion. Int. Water Power Dam Constr. 38 (6), 43–48.
Robinson, K.M., Hanson, G.J., 2001. Headcut erosion research. V. Process. 15.
Shepherd, R., Schumm, S., 1974. Experimental study of river incision. Geol. Soc. Am. Bull. 85 (2), 257–268.
Spurr, K., 1985. Energy approach to estimating scour downstream of a large dam. Int. Water Power Dam Constr. 37 (7), 81–89.
Whipple, K.X., Hancock, G.S., Anderson, R.S., 2000. River incision into bedrock: mechanics and relative efficacy of plucking, abrasion, and cavitation. Geol. Soc. Am. Bull. 112 (3), 490–503.
Wohl, E., Ikeda, H., 1997. Experimental simulation of channel incision into a cohesive substrate at varying gradients. Geology 25 (4), 295–298.
WRA (Water Resources Agency), 2010. A Study on the Mechanisms and Evaluation of Rockbed Erosion After Weir Installation (in Chinese).